Materials Today Bio 26 (2024) 101071

Contents lists available at ScienceDirect

Materials Today Bio

journal homepage: www.journals.elsevier.com/materials-today-bio

A vascularized *in vivo* melanoma model suitable for metastasis research of different tumor stages using fundamentally different bioinks

Rafael Schmid [a,*], Sonja K. Schmidt [b], Stefan Schrüfer [c], Dirk W. Schubert [c], Stefanie Heltmann-Meyer [a], Martin Schicht [d], Friedrich Paulsen [d], Raymund E. Horch [a], Anja K. Bosserhoff [b,1], Annika Kengelbach-Weigand [a,1], Andreas Arkudas [a,1]

[a] *Laboratory for Tissue-Engineering and Regenerative Medicine, Department of Plastic and Hand Surgery, University Hospital of Erlangen, Krankenhausstraße 12, 91054, Erlangen, Germany*
[b] *Institute of Biochemistry, Friedrich-Alexander University Erlangen-Nürnberg, Fahrstraße 17, 91054, Erlangen, Germany*
[c] *Institute of Polymer Materials, Friedrich-Alexander University Erlangen-Nürnberg, Martensstraße 7, 91058, Erlangen, Germany*
[d] *Department of Functional and Clinical Anatomy, Friedrich-Alexander University Erlangen-Nürnberg, Universitätsstraße 19, 91054, Erlangen, Germany*

ARTICLE INFO

Keywords:
Tissue engineering
Bioink
Melanoma
Tumor
Metastasis

ABSTRACT

Although 2D cancer models have been the standard for drug development, they don't resemble *in vivo* properties adequately. 3D models can potentially overcome this. Bioprinting is a promising technique for more refined models to investigate central processes in tumor development such as proliferation, dormancy or metastasis.

We aimed to analyze bioinks, which could mimic these different tumor stages in a cast vascularized arteriovenous loop melanoma model *in vivo*. It has the advantage to be a closed system with a defined microenvironment, supplied only with one vessel—ideal for metastasis research.

Tested bioinks showed significant differences in composition, printability, stiffness and microscopic pore structure, which led to different tumor stages (Matrigel and Alg/HA/Gel for progression, Cellink Bioink for dormancy) and resulted in different primary tumor growth (Matrigel significantly higher than Cellink Bioink). Light-sheet fluorescence microscopy revealed differences in vascularization and hemorrhages with no additional vessels found in Cellink Bioink. Histologically, typical human melanoma with different stages was demonstrated. HMB-45-positive tumors in progression inks were infiltrated by macrophages (CD163), highly proliferative (Ki67) and metastatic (MITF/BRN2, ATX, MMP3). Stainings of lymph nodes revealed metastases even without significant primary tumor growth in Cellink Bioink.

This model can be used to study tumor pathology and metastasis of different tumor stages and therapies.

1. Introduction

Melanoma is a highly malignant skin cancer that has its origin in melanocytes. Even small primary tumors typically can metastasize at an early time point. These metastases can be found in skin but also in lymph nodes, lungs, liver and brain [1]. Advanced stages, where a surgical resection is no longer indicated, are targets for novel drugs. With these, prognosis of patients has improved over the last decade. Nevertheless, drug resistances are still a prominent problem. Hence, there is a huge demand for highly complex models to study molecular processes and evaluate and improve therapies.

Tissues and organs are complex, hierarchical structures containing multiple cell types depending on vascularization with increasing size. Similarly, tumors and their microenvironment also consist of various cells and rely on vascularization and angiogenesis to prevent necrosis of larger tumor masses. This tumor microenvironment has been shown to play a crucial role in tumor promotion and in drug receptiveness [2,3]. Hence, complex 3D models have been created to mimic the microenvironment as accurately as possible. These often make use of hydrogels and, in recent years, also printable hydrogels for biofabrication, and offer interesting insight into phenotypical changes caused by the microenvironment [4]. Printable hydrogels with cells, the so-called bioinks, are used for creating the desired structures in a precise and controllable manner. The hydrogel should ideally resemble the extracellular matrix in structure, composition, and biomechanical properties.

* Corresponding author.
E-mail address: rafael.schmid@uk-erlangen.de (R. Schmid).
[1] equal contribution.

https://doi.org/10.1016/j.mtbio.2024.101071
Received 12 February 2024; Received in revised form 21 April 2024; Accepted 25 April 2024
Available online 27 April 2024

List of abbreviations

Alg/HA/Gel	alginate/hyaluronic acid/gelatin bioink
AV	arteriovenous
ATX	autotaxin
BRN2	POU domain, class 3, transcription factor 2
DAPI	4′,6-diamidino-2-phenylindole
DMA	dynamic mechanical analysis
HMB	Human Melanoma Black
LSFM	light-sheet fluorescence microscopy
MIA	Melanoma Inhibitory Activity
MITF	Microphthalmia-associated transcription factor
MILNs	*Lymphonodi iliaci mediales*
MMP3	matrix metalloproteinase-3
PMEL	premelanosome protein
SiLN	*Lymphonodus subiliacus*

Therefore, they have to be adapted to the desired application. One standard material often used for cancer models is Matrigel, a basement membrane-like mixture of type IV collagen, laminin, entactin, heparan sulfate proteoglycans, and various growth factors. It allows ideal tumor interaction including adhesion and remodeling. Other commercial products, like Cellink Bioink, are more defined and consist of selected components like in this case nanocellulose and alginate for crosslinking. This combination does not allow active receptor interaction with mammalian cells. Hence other bioinks, that are more favorable for mammalian cells in terms of anchorage, interaction and remodeling, incorporate besides alginate further ECM-derived molecules like gelatin [5] or hyaluronic acid [6]. Recently, a combination of all of these components as a bioink has been proven to be suitable as complex *in vivo* model [7].

This *in vivo* model combats one of the major challenges in tissue engineering, the lack of adequate vascularization in larger constructs. The arteriovenous (AV) loop model has been proven to be a very effective option to vascularize a 3D scaffold in a controlled manner *in vivo* [8]. In this rat model, the femoral artery and vein are anastomosed into an AV loop by interposing a venous graft from the contralateral side of the animal. The resulting vascular loop is put into a chamber that is filled with a hydrogel or bioink. In suitable hydrogels, this vascular loop starts neovascularization by vascular sprouting into the hydrogel over the course of a few weeks, ensuring supply of incorporated cells with nutrients. This makes the AV loop an interesting option also for tissue engineering as the patient's body could be used as a bioreactor to vascularize a tissue-engineered construct. Bioprinting increases the controllability of the AV loop model e. g. through precise positioning of different cells of the tumor microenvironment or macroporous structures.

With this study, we evaluated the influence of the three different bioinks Matrigel, Cellink Bioink, and Alg/HA/Gel on the growth of primary melanomas and metastases in the AV loop model to further establish it as a robust tumor model.

2. Methods

2.1. Cell culture

For this study, the melanoma cell line Mel Im was used. It is of metastatic origin and was cultivated in DMEM low glucose (Sigma-Aldrich, St. Louis, MO, USA) with L-glutamine (2 mM, Sigma-Aldrich), 10 % FCS Superior (standardized fetal bovine serum, Biochrom GmbH, Berlin, Germany), and penicillin/streptomycin (100 U ml^{-1}, 0.1 mg ml^{-1}, Sigma-Aldrich). The incubator was set to 5 % CO2 at 37 °C. Medium was changed three times per week.

2.2. Ink composition

Matrigel Basement Membrane Matrix (Corning, Inc., Corning, NY, USA) was used undiluted according to the manufacturer's protocol. Cellink Bioink (Cellink, BICO Group, Gothenburg, Sweden) was diluted 10 + 1 with cell culture medium according as indicated by the manufacturer. Alg/HA/Gel was created as previously published [7]. 0.5 % m v^{-1} VIVAPHARM Alginate PH 176 (JRS PHARMA GmbH & Co. KG), 3 % m v^{-1} gelatin from porcine skin (gel strength ≈ 300 g Bloom, Type A, Sigma-Aldrich), and 0.1 % m v^{-1} hyaluronic acid (1–2 MDa, CarboSynth Ltd, Compton, UK) were dissolved in PBS without Ca^{2+} and Mg^{2+} (Sigma-Aldrich) at 37 °C.

2.3. Rheology

The elastic and viscous properties of the three non-crosslinked inks were measured as previously described [9]. A DHR-3 rheometer (TA Instruments, New Castle, DE, USA), equipped with a 20-mm plate-plate geometry (for Alg/HA/Gel) or a 40-mm plate-plate geometry (for Cellink Bioink) or a 40-mm cone-plate (1.99° for Matrigel) and a Peltier element for temperature control, was used. 200 μl of Alg/HA/Gel or 850 μl of Cellink Bioink and Matrigel, the uncured inks were added between the plate-plate geometry. For Alg/HA/Gel, the temperature of the rheometer was set to 37 °C. Then, the ink was cooled down to 15 °C at 2 °C min^{-1} and maintained for 6 min. Matrigel was thawed at 4 °C over night heated for 6 min with a linear temperature ramp from 4 °C to 20 °C and measured after 15 min at 20 °C. Cellink Bioink was measured at 25 °C respectively. Oscillation experiments were performed, in which the storage modulus G′ and the loss modulus G″ as well as the value of complex viscosity were measured/calculated using a frequency sweep (0.1–100 rad s^{-1}). The ratio of G″ to G′ is calculated as $\tan\delta = G''/G'$. For better readability, the value of complex viscosity is referred to as complex viscosity in the following manuscript. Three technical replicates were composed from one batch of ink.

2.4. Printability assays

The printability of the three inks was additionally evaluated using a filament fusion and a grid structure test according to Hazur et al. [10] using a Cellink Inkredible+ (Cellink).

Cellink Bioink was printed at RT. To achieve printability of Matrigel and Alg/HA/Gel, 2 ml Matrigel was transferred into a 3-ml cartridge and warmed to 20 °C for 6 min in a water bath and printed while 2 ml Alg/HA/Gel was cooled to 15 °C for 6 min and then printed as follows.

The meander-shaped filament fusion test with decreasing distance between adjacent strands makes it possible to evaluate the printing resolution. In short, cylindrical nozzles with 250-μm inner diameter (25G, Vieweg GmbH, Kranzberg, Germany) were used to print 20 mm long parallel strands with 2–0.5 mm distance. The minimal distance is evaluated where strands do not fuse. This distance is categorized as A (0.5 mm), B (0.75 mm), C (1 mm), D (1.5 mm), or E (2 mm). This experiment was performed in technical triplicates.

In the grid structure test the merging of two perpendicular strands is measured. For this, grids with 10 mm length and 6 strands each direction were printed. At five crossing points, the diagonals of the strands were measured. The ideal diameter without merging of strands is 354 μm using a 250-μm nozzle. The diagonal crossing ratio (DCR) is then calculated as the ideal diameter divided by the measured diameter. Hence, values closer to 1 are better. The experiment was performed in 5 technical replicates.

2.5. DMA

The elastic and viscous properties of the three crosslinked hydrogels were measured as previously described [7,11] using dynamic mechanical analysis (DMA). In short, 2 mm high films were prepared and

measured after overnight incubation at 37 °C in complete cell culture medium. A DHR-3 rheometer (TA Instruments, New Castle, DE, USA) was equipped with a 20-mm plate-plate geometry and set to oscillating compression mode. An axial pre-force of 0.1 N was applied and the tests were performed at 37 °C. A range of at least 0.1–10 rad s^{-1} was covered. Average values and standard deviations were calculated from at least three measurements of technical replicates. Both moduli (storage modulus E′ and loss modulus E″) were determined.

2.6. Scanning electron microscopy

The prepared hydrogel samples (Matrigel, Cellink Bioink and Alg/HA/Gel) were postfixed in ITO's fixative containing 25 % paraformaldehyde, 25 % glutaraldehyde, 0.1 M sodium cacodylate (all Carl Roth GmbH & Co KG, Karlsruhe, Germany) and picric acid. Afterwards, they were dehydrated in an ascending series of acetone (Sigma-Aldrich). Afterwards the samples were critical point dried by using the Leica EM CPD300 system (Leica Mikrosysteme GmbH, Vienna, Austria). The hydrogel samples were carefully separated to expose the inside and fixed on SEM pin stubs (Ted Pella Inc., Redding, CA, USA) by use of double-sided 25-mm adhesive carbon tabs (Plano GmbH, Wetzlar, Germany) under using a desiccator and coated with a 21-nm layer of gold using the sputter Leica EM ACE200 system (Leica Mikrosysteme GmbH). Finally, all hydrogel samples were examined using a JEOL scanning electron microscope (JSM-IT 300LV, JEOL Germany GmbH, Freising, Germany). Pore size and count were quantified manually using Fiji/ImageJ 1.53c [12] in three ROIs of 1365 μm^2. Representative images were sharpened with ImageJ for better visualization of the microscopic structures.

2.7. Ki67 staining in vitro

To evaluate the dormant phenotype of the melanoma cell line Mel Im [13] *in vitro*, a Ki67 staining was performed. Mel Im (1×10^6 ml^{-1}) were encapsulated in the three different gels and crosslinked (Alg/HA/Gel and Cellink Bioink 10 min, 100 mM $CaCl_2$; Matrigel 30 min at 37 °C) and afterwards covered with medium. A 2D control was seeded into a 48-well plate. On day 3, the samples were fixed using formaldehyde (Carl Roth GmbH & Co. KG) for 10 min, permeabilized (0.25 % Triton X-100 in HBSS) and labeled with a Ki67 antibody (1:100, clone SP6, RBK027-05, Zytomed Systems GmbH, Bargteheide, Germany) for 1 h. And isotype control with the same IgG1 concentration was performed. Afterwards, an anti-mouse Alexa 488 (Thermo Fisher Scientific Inc., Waltham, MA, USA) was used (30 min). Counterstaining was performed with 4′,6-diamidino-2-phenylindole (DAPI) (1 μg ml^{-1}, Thermo Fisher Scientific Inc., 6 min). Images were taken on an Olympus IX83 with cellSens Software V1.16 (Olympus Corporation, Tokyo, Japan) and the background reduced using ImageJ for better visualization.

2.8. In vivo implantation

In this study, the microsurgical AV loop model (Fig. 1) was the main technique used to implant the hydrogels into male immune-deficient RNU rats (Crl:NIH-*Foxn1*^{rnu}, Charles River Laboratories, Wilmington, MA, USA). The surgery was performed as described in earlier publications [7,14]. These experiments were approved by the Animal Care Committee of the University Erlangen-Nürnberg and the Government of Unterfranken, Germany (license number 55.2-2532-2-718). Animals were kept in a standardized environment (light/dark cycles of 12 h, 20–22 °C, RH 46–48 %) in individually ventilated cages.

The rats (body weight between 315 g and 445 g) were anesthetized using isoflurane (CP-Pharma, Burgdorf, Germany). Medication was given intravenously (1 mg kg^{-1} meloxicam (Boehringer Ingelheim Vetmedica GmbH, Ingelheim am Rhein, Germany), butorphanol (1.5 mg kg^{-1}, CP-Pharma), enrofloxacin, (7.5 mg kg^{-1}, Bayer, Leverkusen, Germany)). The rats were placed on their backs and a venous graft of the right femoral vein was harvested and flushed using a 50 IU ml^{-1} heparin

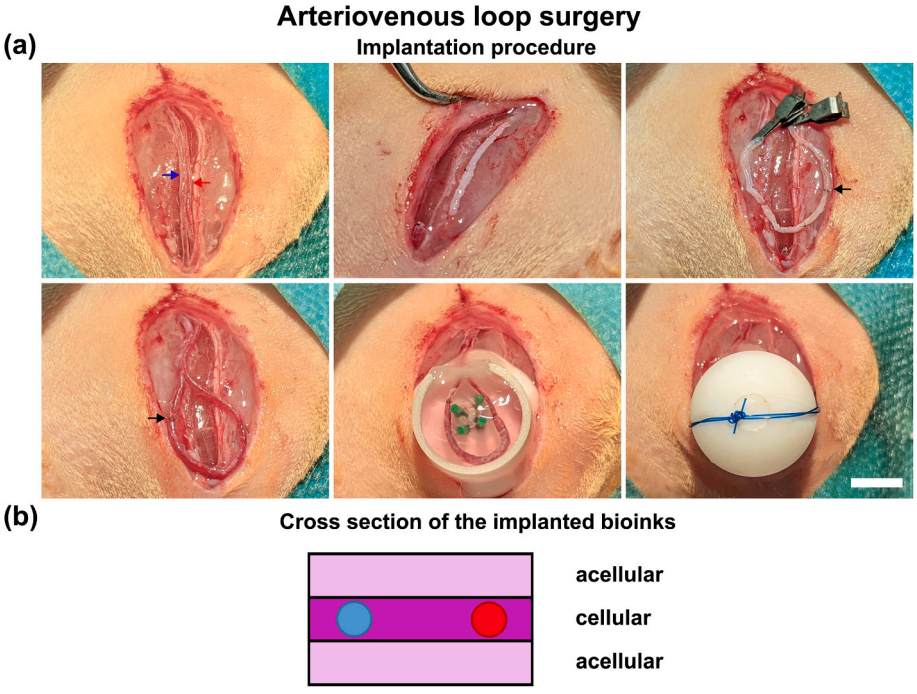

Fig. 1. Arteriovenous loop surgery: (a): *upper left:* opened surgical site with exposed vessels (red arrow artery, blue arrow vein) vessel diameter approx. 1 mm, *upper middle:* lifting of the venous graft in the other leg after flushing with heparin solution, *upper right:* first end-to-end anastomosis (11-0 sutures, black arrow) after flushing with heparin and attaching the micro clamps between artery and vein graft and preparation of the second between vein graft and vein, *lower left:* patent AV loop, second end-to-end anastomosis completed (black arrow) and clamps removed, *lower middle:* AV loop embedded in cast Alg/HA/Gel hydrogel in PTFE chamber, entrance is closed with fibrin, green pins for stabilization, *lower right:* closed chamber attached to the muscle, before closing the skin; scale bar = 5 mm; **(b)**: casting schematics with cellular and acellular layers within the chamber; the cellular layer is located around the AV loop vessels to facilitate cell survival.

solution (ratiopharm GmbH, Ulm, Germany). The distal end of the graft was connected (interrupted knots, 11-0 nylon sutures; Ethicon, Inc, Somerville, NJ, USA) to the left femoral artery and the proximal end connected to the left femoral vein via end-to-end anastomosis to the AV loop. A PTFE chamber with an inner diameter of 10 mm and an inner height of 6 mm was used which was sutured onto the muscle.

The chamber was filled with the different bioinks according to the different groups below. 1×10^6 Mel Im cells were used in each group in the middle layer. The middle layer was chosen as cellular layer as it is closest to the vessel, therefore provides the best support with nutrients and highest chance of cellular survival. Due to different shrinking of the inks during crosslinking, different voluminal were used to fill the chamber. The chamber entrance was closed with clot human fibrin (Baxter, Deerfield, IL, USA). The chamber and the wounds were closed. Enoxaparin sodium (10 mg kg^{-1}, Sanofi S.A., Paris, France) was administered two days post-operatively, meloxicam (1 mg kg^{-1}) for 7 days, and enrofloxacin for 5 days. The chambers were explanted after 4 weeks.

Matrigel Basement Membrane Matrix was used in the first group (n = 6). 250 μl were cast into the chamber and gelled for 10 min. The loop was positioned on top and 100 μl Matrigel together with the cells were added. After 10 min, the last layer of 250 μl Matrigel was added.

Cellink Bioink was also used in a layered system (n = 7). Before implantation, cylinders of 160 μl Cellink Bioink were cast (diluted 10 + 1 with medium) and crosslinked with the included crosslinker for 10 min. This cylinder was placed within the chamber. The loop was placed on top and 157 μl bioink together with the cells were added and crosslinked. The chamber was filled with Cellink Bioink without cells and again crosslinked.

Alg/HA/Gel was implanted as previously published [7]. This bioink was already found to be suitable for the *in vivo* melanoma model and the data is used for comparison (n = 9). In short, the hydrogel was used in a cast sandwich technique, first with a layer of pre-crosslinked hydrogel (600 μl in a 12-well and punched to 10 mm diameter), then, together with the loop, a layer of hydrogel (300 μl), with cells, that was crosslinked in situ, then another pre-crosslinked layer on top.

2.9. Measurement of the MIA serum concentrations

The human Melanoma Inhibitory Activity (MIA) level in the blood serum was measured as a tumor marker. Once per week, the rats were anesthetized, blood was taken through a lateral tail vein and collected using S-Monovette 1.1-ml Z-Gel tubes (SARSTEDT AG & Co. KG, Nümbrecht, Germany). After centrifugation, the serum was frozen and then used in duplicates for the MIA ELISA according to the manufacturer's protocol (Roche, Holding AG, Basel, Switzerland). A four parameter rodbard function was used to evaluate the standard.

2.10. Staining and imaging of constructs

To visualize the vascularization, an injection with fluorescently labeled anti-CD31 antibodies (1 ml, 0.05 mg ml^{-1}, labeled with Alexa Fluor 647, Clone TLD-3A12, MCA1334A647, Bio-Rad Laboratories, Inc., Hercules, CA, USA) was performed as previously published [7] and the chamber explanted after 20 min.

The explants were fixed with 4 % formaldehyde for 8–12 h at 4–8 °C. Bleaching was performed using 1.75 % H_2O_2 (Carl Roth GmbH & Co KG) and 5 % DMSO (Sigma-Aldrich) in PBS. Samples were incubated in the bleaching buffer for 4 h at 4–8 °C. Afterwards, tissue dehydration and optical clearing using ethyl cinnamate (Sigma-Aldrich) was performed as described previously [7,15,16]. The cleared explants were imaged using light-sheet fluorescence microscopy (LSFM).

LSFM of optically cleared AV loops was performed with an Ultramicroscope II (LaVison BioTec GmbH, Bielefeld, Germany) including an Olympus MVX10 zoom body, a LaVision BioTec Laser Module, and an Andor Neo sCMOS Camera with a pixel size of 6.5 μm, and 2 × detection optics with a numerical aperture (NA) of 0.5. The optical zoom was adjusted to 0.8 × , 1 × , or 2 × and the light sheet thickness was set in a range of 4 μm–10 μm.

Visualization of general tissue autofluorescence was conducted either via a 488-nm optically pumped semiconductor laser with detection filters at 525/50 nm or excited at 561 nm via an optically pumped OPSL and emitted signals detected at 620/60 nm. A 647-nm diode laser was used with the filter 680/30 nm was used for CD31-AF647. Generated data were collected with ImspectorPro software version 5.1.304 and processed with Imaris software version 9.1 (Bitplane AG, Zürich, Switzerland).

2.11. Histology

After LSFM, the constructs and explanted lymph nodes were embedded into paraffin and cut into 5-μm histological sections using a microtome (Leica Microsystems, Wetzlar, Germany). Several histological HE (Leica Autostainer XL, Leica Microsystems), and Human Melanoma Black (HMB-45) (ENZ-C34930, Enzo Life Sciences, Inc., Farmingdale, NY, USA; VENTANA BenchMark ULTRA, Roche) stainings were done by the local pathological institute (University Hospital Erlangen). HMB-45 binds to premelanosome protein (PMEL) in melanoma. The stainings of sections of chambers were quantified semi-automatically using the LAS (version 4.12.0, Leica Microsystems) or Fiji/ImageJ, and the tumor area was set in relation to the total tissue area without the remaining hydrogel (measured manually in adjacent HE stainings). Per animal, at least two sections of the chamber were quantified and the means of the tumor ratio were calculated.

For the metastases in the lymph nodes, ImageJ was used to manually count the metastatic clusters, and to measure the area of the organs (2 sections per animal and organ, Cellink Bioink n = 6).

A Ki67 antibody (1:200, clone SP6, RBK027-05, Zytomed Systems GmbH) was used to visualize proliferative cells. A citrate buffer pH 6 (Dako Target Retrieval, Agilent, Santa Clara, CA, USA) was used for antigen retrieval. For staining, the CSA II Biotin-Free Tyramide Signal Amplification System (Dako, Agilent) was used according to the manufacturer's instructions. Counterstaining was performed with DAPI.

CD163 staining was performed as previously published [17]. In short, anti-CD163 (1:200, clone ED2, MCA342GA, Bio- Rad) was used after pretreatment with pronase (Sigma-Aldrich). The detection system was a polymer kit (ZytoChem Plus AP, Zytomed Systems GmbH). Sections were counter-stained with Mayer's hemalum (Merck KGaA, Darmstadt, Germany).

For the autotaxin (ATX) staining, a polyclonal anti-ENPP2/ATX antibody was used (1:100, ab140915, abcam, Cambridge, UK). A permeabilization buffer was used (Invitrogen, Waltham, MA, USA). Again, a polymer kit was used for staining with Mayer's hemalum as counterstaining.

Matrix metalloproteinase-3 (MMP3) staining was performed as previously described [18]. In short, an anti-MMP3 antibody (1:60, SAB4501892-100, Sigma-Aldrich) was used after incubation in citrate buffer (pH 6). The detection system was a peroxidase/DAB kit (Dako, EnVision, Agilent).

Microphthalmia-associated transcription factor (MITF) and BRN2 double staining was performed using secondary fluorescent antibodies. A TRIS-EDTA puffer (pH 8) was used for antigen retrieval. An anti-MITF antibody (1:80, clone SPM290, ab233928, abcam) and a polyclonal anti-BRN2 antibody (1:100, ab137469, abcam) were used. As secondary antibodies, Alexa Fluor 488 anti-mouse and Alexa Fluor 647 anti-rabbit (both 1:200, invitrogen) were used with DAPI as counter-staining.

Images were taken on an Olympus IX83 with cellSens Software V1.16 (Olympus Corporation). For MITF and BRN2 stainings, a background reduction, sharpening and contrast enhancement was performed using ImageJ.

2.12. Statistics and figures

Statistical analysis was performed by using GraphPad Prism 8.1.2 (GraphPad Software, La Jolla, CA, USA). Differences between groups were analyzed using the following tests where appropriate: Grubb's test for outliers, Shapiro-Wilk normality test followed by Kruskal-Wallis test due to non-parametric distribution of samples and Dunn's multiple comparisons test for tumor area, CD163 signal and MIA ELISA; Shapiro-Wilk normality test followed by paired *t*-test for metastasis rates within the Cellink Bioink group. Significant p-value was set to ≤ 0.05.

Figures show a box plot with whiskers or dot plots and were created with GraphPad Prism. Depicted microscopic images were arranged and edited with Inkscape 1.2. Fig. 9 was created with BioRender.com.

3. Results

3.1. Bioinks have different shape-fidelity

In this study, the printability in extrusion-based bioprinting approaches of three different non-crosslinked inks was evaluated. A filament fusion test and a grid structure test were performed (see Fig. 2).

Cellink Bioink and Alg/HA/Gel performed similar in the filament fusion test with fusions starting below a strand distance of 0.75 mm, making both category B inks. Matrigel performed significantly worse with a visibly inhomogeneous strand and fusion at 1.5 mm, resulting in category E.

The grid structure test supports this categorization. Here, printing of Cellink Bioink and Alg/HA/Gel resulted in reproducibly defined grids with proper shape-fidelity. Matrigel showed massive merger of strands, which resulted in a less-defined grid. Quantification of the crossing points (Fig. 2(b)) revealed a diagonal crossing ratio (DCR) of 0.22 ±

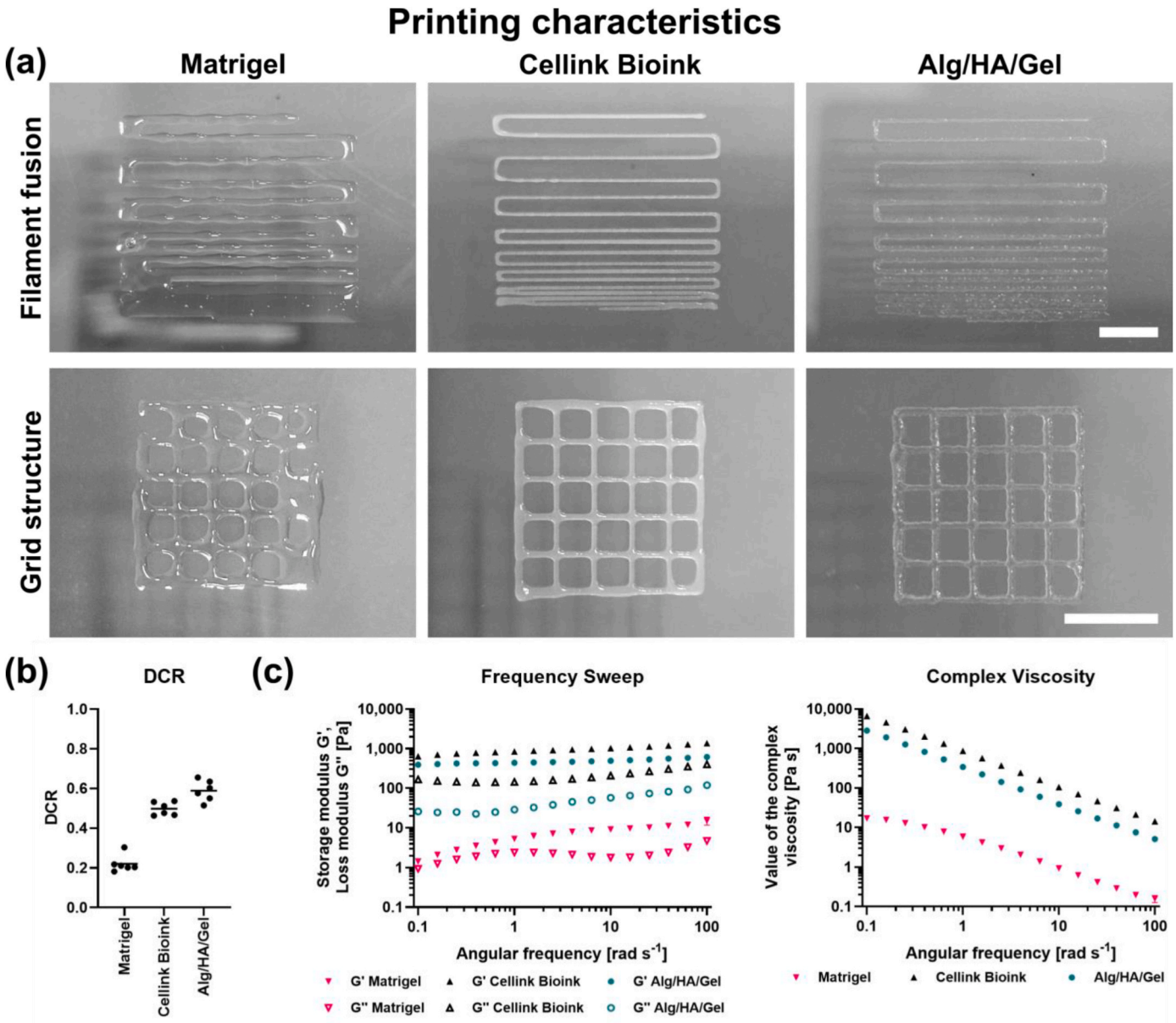

Fig. 2. Printing characteristics of three inks: (a): filament fusion test and grid structure test of Matrigel, Cellink Bioink, and Alg/HA/Gel, scale bars = 5 mm; **(b)**: DCR quantification of the grid structure test of the three inks, data shown as mean and replicates; **(c)**: rheological evaluation of the three inks (storage modulus G', loss modulus G'' and value of complex viscosity of Alg/HA/Gel was published previously [9]); data shown as mean ± SD of technical replicates.

0.04 for Matrigel, 0.50 ± 0 03 for Cellink Bioink and 0.59 ± 0.05 for Alg/HA/Gel, attesting Matrigel the worst and Alg/HA/Gel the best shape-fidelity.

Rheological evaluation (Fig. 2(c)) of the non-crosslinked inks showed that all inks have viscoelastic properties. More precisely, the elastic properties (storage modulus G') of Cellink Bioink and Alg/HA/Gel are larger than their viscous properties (loss modulus G''), confirming their good shape-fidelity. In the frequency sweep performed, Cellink Bioink had a G' of 846.5 ± 41.9 Pa and a G'' of 144.2 ± 12.2 Pa (tan δ = 0.17), Alg/HA/Gel had a G' of 439.3 ± 19.3 Pa and a G'' of 28.8 ± 1.7 (tan δ = 0.06) at 1 rad s^{-1}. Matrigel is the least elastic and least viscous material with a G' of 5.3 ± 0.3 Pa and a G'' of 2.4 ± 0.1 Pa at printing conditions (tan δ = 0.45). All bioinks show shear-thinning behavior as the value of complex viscosity decreases with angular shear frequency. Rheological measurements of Alg/HA/Gel were already published [9] but added here for direct comparison.

3.2. Hydrogels from inks have different stiffness and microporous structure

Before implantation into the *in vivo* model, the elastic properties of the hydrogels used were analyzed via DMA (Fig. 3). Here, the hydrogels, Matrigel, Cellink Bioink, and Alg/HA/Gel showed mainly elastic properties as their storage modulus E' was much greater than the loss modulus E″ (E′≫E″) at 37 °C. The storage modulus of Alg/HA/Gel was already published [7] but the data added here for direct comparison. For

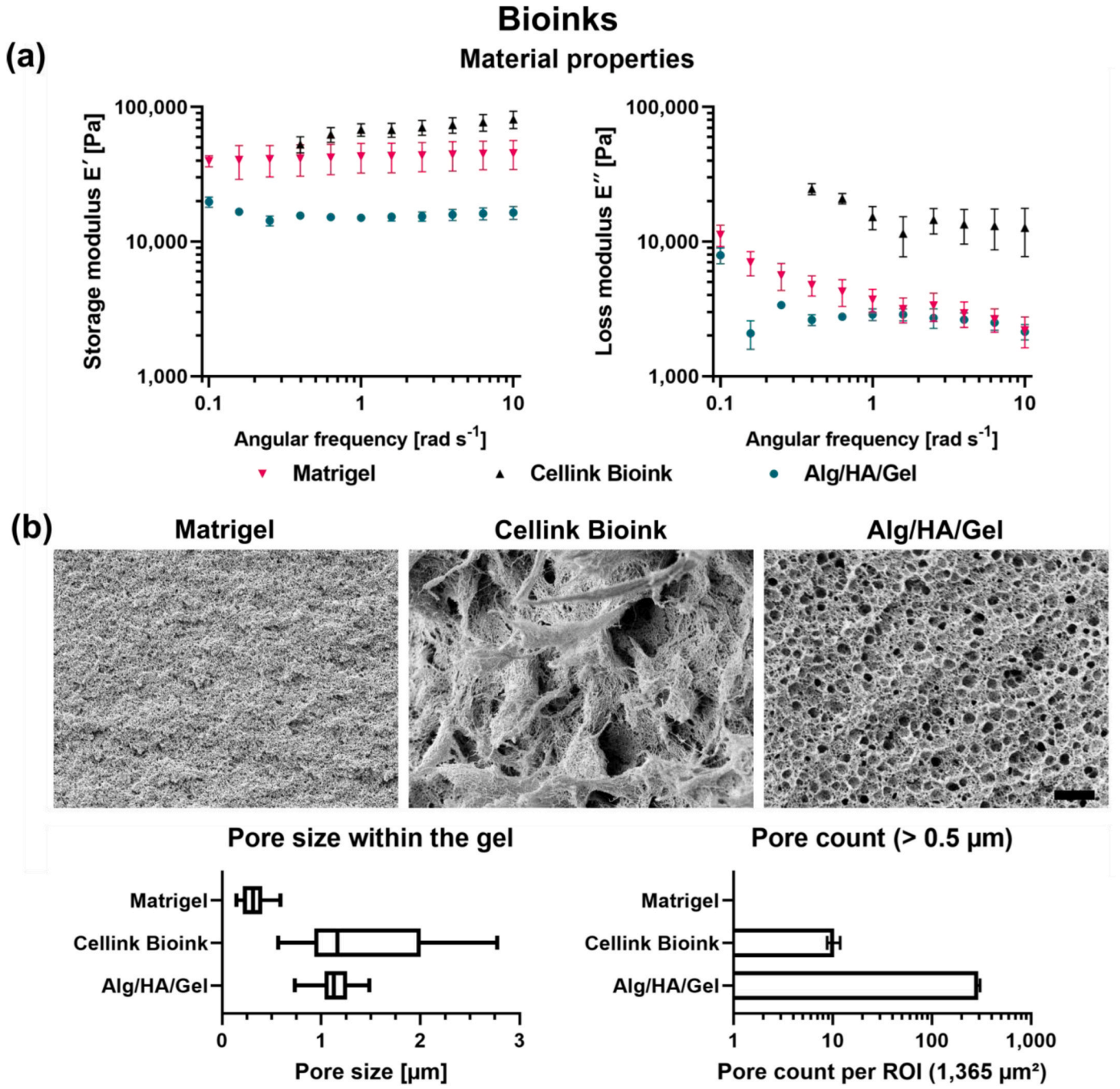

Fig. 3. Material properties of three inks: (a): storage modulus E' and loss modulus E″ of Matrigel, Cellink Bioink, and Alg/HA/Gel (E' of Alg/HA/Gel was published previously [7]); data shown as mean ± SD of technical replicates; **(b)**: scanning electron microscopy characterization of the inside of the hydrogels with quantification; scale bar = 5 µm; pore size shown as box plot (Tukey) of 3 ROIs, pore count per ROI shown as mean ± SD of pores > 0.5 µm.

evaluation, 1 rad s^{-1} was chosen as reliable data point in the low-frequency range, which is relevant for cells. The storage moduli differed to a great extent and Alg/HA/Gel's E' was with 15.1 ± 0.9 kPa at 1 rad s^{-1} lower than the other two. For Matrigel 43 ± 10.6 kPa and for Cellink Bioink 67.9 ± 7.3 kPa were measured.

The results of the SEM analysis show different microscopic structures of the insides of the hydrogels. Matrigel has a smoother structure than Alg/HA/Gel and Cellink Bioink. Micro/nanocellulose fibers can also be seen in Cellink Bioink within the alginate. The apparent impression of the ink structure is also supported by the measured pore size in the gel. This is 1.42 ± 0.65 μm for Cellink Bioink, 1.14 ± 0.18 μm for Alg/HA/Gel and the smallest for Matrigel with 0.31 ± 0.11 μm. When determining the number of pores per ROI, only pores with a diameter > 0.5 μm were taken into account. Under these conditions, two pores could be counted in 3 ROIs of Matrigel, while again fewer pores were present in Cellink Bioink than in Alg/HA/Gel (10.33 ± 1.53 vs. 291.67 ± 15.04 per ROI). The pores in Alg/HA/Gel appear to be interconnected. This is not the case for Cellink Bioink, which is denser.

3.3. Varying proliferation in vitro depending on bioink choice

To evaluate the dormant phenotype of the melanoma cell line Mel Im *in vitro*, a Ki67 staining was performed (Fig. 4).

After three days in Cellink Bioink, cells did not proliferate and reduced their Ki67 expression. Within the other hydrogels, cells were able to proliferate with a maintained high Ki67 expression. Colonies in Alg/HA/Gel were spherical without spreading into the gel while in Matrigel, cells were able to migrate and spread. Cells escaping the hydrogel due to degradation proliferate non-hindered in all the different bioinks, making the dormancy phenotype in Cellink Bioink reversible.

3.4. Varying tumor growth in vivo depending on bioink choice

The bioinks were implanted *in vivo* into the cast vascularized AV loop rat model using the melanoma cell line Mel Im. After four weeks, the implantation chambers were explanted. For the analysis, for Matrigel n = 6, Cellink Bioink n = 7, and Alg/HA/Gel n = 9 animals were used. All those animals survived the surgery and showed good wound healing with typical phenotype.

The implantation of Mel Im with Matrigel and Alg/HA/Gel resulted in substantial tumor growth to varying extent (Fig. 5). In Matrigel, 6 of the 6 animals developed a solid tumor that grew out of the implantation chamber's entrance while this did not happen in any of the Cellink Bioink animals. In 7 of the 9 Alg/HA/Gel animals a solid tumor also grew out of the chamber. Examples of the explants are shown in Fig. 5 (a).

HE, HMB-45 and Ki67 histological stainings revealed highly proliferative melanomas in different sizes in the various explants for Matrigel and Alg/HA/Gel. With one exemption, which was identified as outlier, the Cellink Bioink animals did not develop solid tumors that were larger than 7 % of the whole tissue (4 % mean). Quantification of the tumor sizes is shown in Fig. 5(c). Here, data of Alg/HA/Gel [7] has been added for better comparison. The range in the Matrigel group was 20–86 % (51 % mean). The range in the Alg/HA/Gel group was 2–96 % (27 % mean). The Matrigel animals' tumors were significantly larger than the Cellink Bioink animals' tumors. There was no significant difference between the Matrigel and the Alg/HA/Gel group.

The tumors were mainly clustered around the large AV loop vessels and proliferated from this origin (detailed pictures can be seen in Fig. 6). With increasing tumor mass in the Matrigel and the Alg/HA/Gel group, the vessel diameters decreased. Depending on the size of the tumors, remaining hydrogels can be detected. Histologically, various hemorrhages can be seen. In contrast, in the Cellink Bioink group without the outlier, neither large tumor masses nor compression of the vessels was detected. Smallest proliferative tumor masses around the vessels were seen. The cells deeper within the hydrogel were not able remodel the matrix and proliferate. Nevertheless, in proximity to the loop, long-term survival of those cells was observed. Furthermore, metastatic cells can

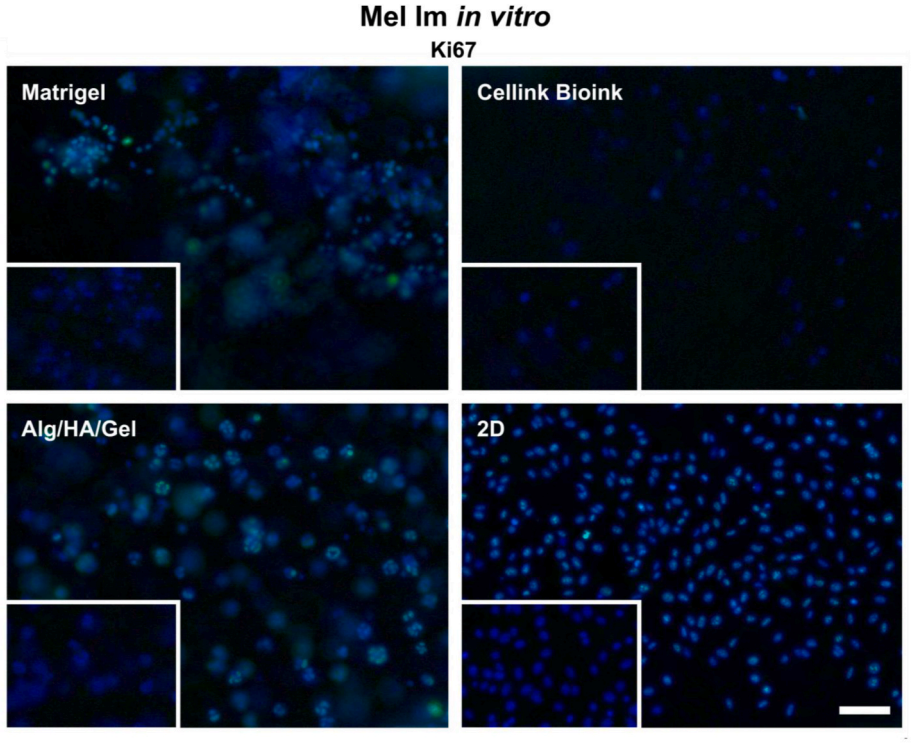

Fig. 4. Melanoma cells *in vitro* with the three different bioinks: Ki67 stainings (green, DAPI in blue) of Mel Im embedded into the hydrogels show a decreased expression after 3 days in culture in Cellink Bioink compared to the other gels Matrigel and Alg/HA/Gel and the 2D culture; isotype controls are shown in the smaller boxes; scale bars = 100 μm.

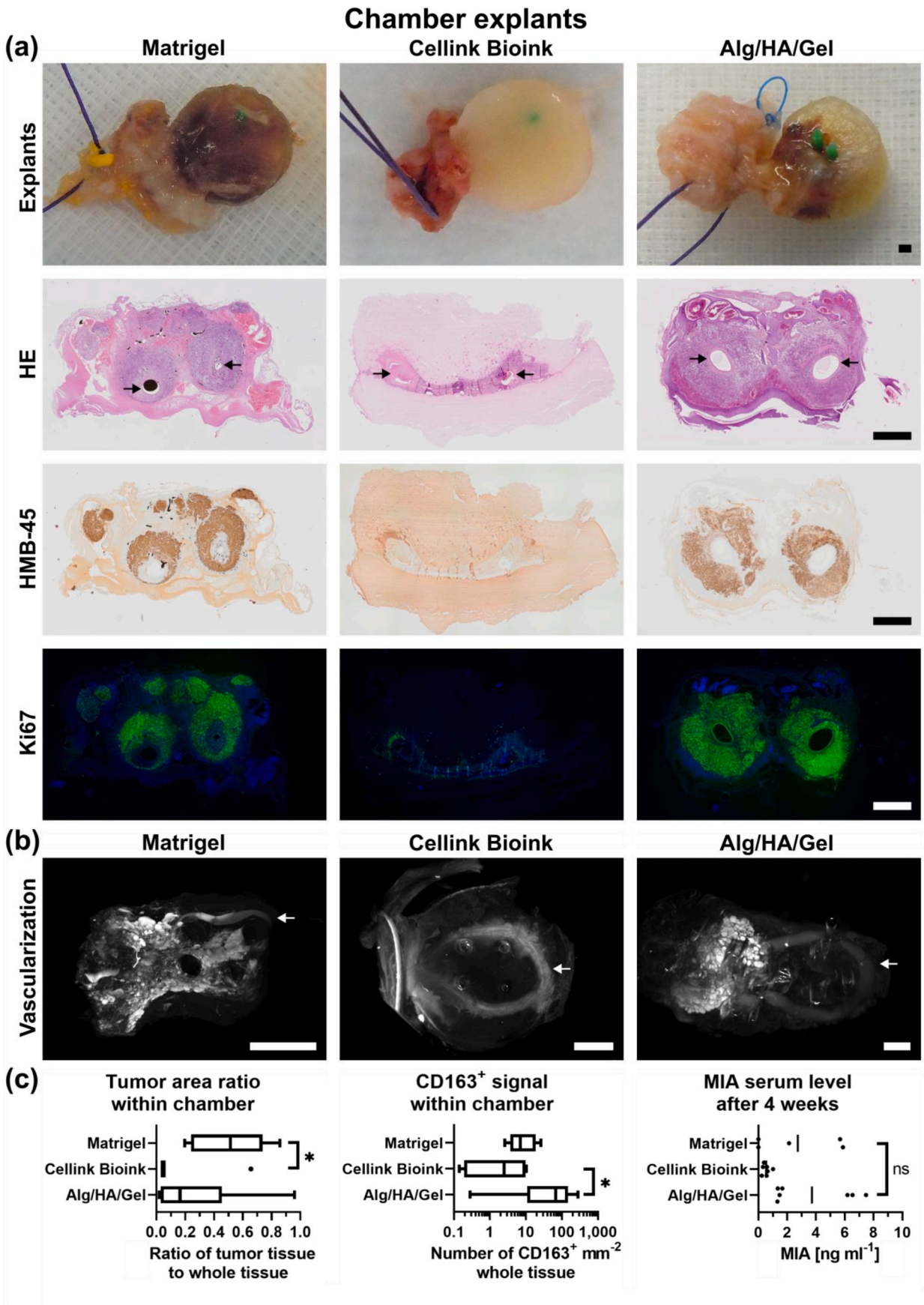

(caption on next page)

Fig. 5. Chamber explants with the three different bioinks: (a): explants and histology (HE, HMB-45 [brown], Ki67 [green]) of representative samples of the groups Matrigel, Cellink Bioink, and Alg/HA/Gel, arrows point at loop vessels, scale bars = 1 mm; **(b)**: vascularization of representative explants visualized via light-sheet fluorescence microscopy for CD31, the chamber entrance is on the left side, arrows point at loop vessels, scale bars = 2 mm; **(c)**: quantification of the tumor area ratio, the CD163-positive macrophages per mm^2 (tumor area of Alg/HA/Gel was already published [7] and added here for direct comparison) of histological sections within the chamber shown as box plot (Tukey) with mean of ≥2 sections of biological replicates, *p ≤ 0.05 (Grubb's test for outliers, Shapiro-Wilk normality test followed by Kruskal-Wallis test and Dunn's multiple comparisons test) and MIA serum levels after 4 weeks shown as individual values plus mean of the group. *p ≤ 0.05 (Shapiro-Wilk normality test followed by Kruskal-Wallis test and Dunn's multiple comparisons test), (MIA levels of Alg/HA/Gel were already published [7] and added here for direct comparison).

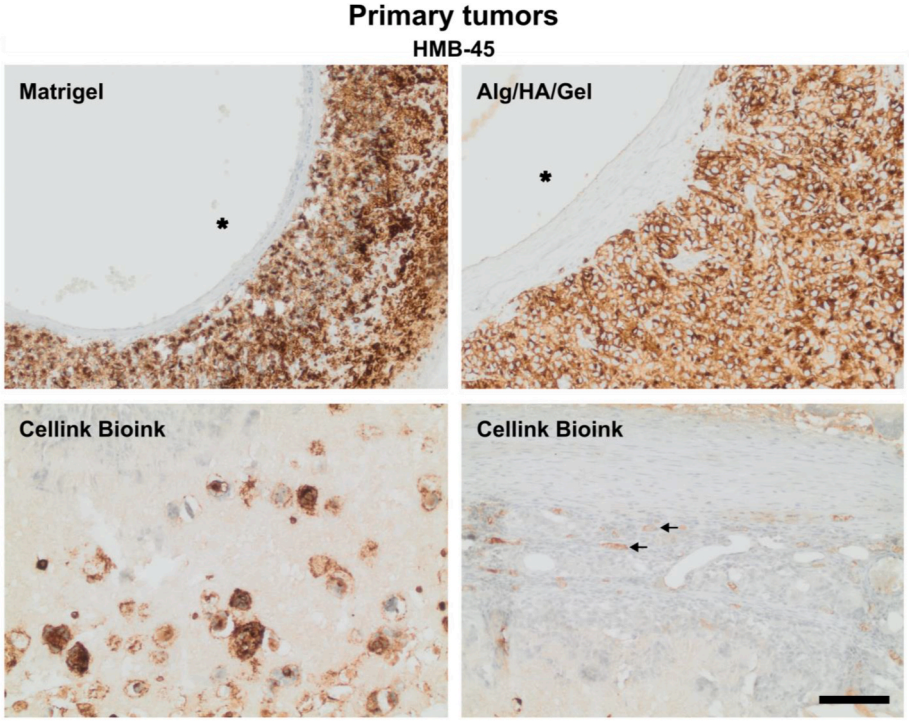

Fig. 6. Comparison of the primary tumor growth between the Matrigel, Cellink Bioink, and Alg/HA/Gel groups: Tumors (HMB-45-positive, brown) in Matrigel and Alg/HA/Gel formed mainly around the AV loop vessel, small metastatic colonies were seen in Cellink Bioink around the AV loop vessel (asterisks mark the lumens, pictures of two exemplary animals); arrows point at exemplary metastatic cells in the vessels and the endothelium; scale bar = 100 μm.

be found in the vessels and their epithelium of these explants.

The tumors showed the typical pathophysiological microenvironment. The large vessels were surrounded by connective rat tissue, as were some tumors. The explants were infiltrated with CD163-positive macrophages, quantified in Fig. 5(c). Their count in Alg/HA/Gel (85.4 $CD163^+$ mm^{-2} mean) was significantly higher than in Cellink Bioink (4.3 $CD163^+$ mm^{-2} mean). The Matrigel group (10.5 $CD163^+$ mm^{-2} mean) was in between without significant differences. Macrophages were also found within the Matrigel and Alg/HA/Gel gel without direct contact to the grown tissue.

Via light-sheet fluorescence microscopy for CD31, the vascularization of the explants was vizualized as displayed in Fig. 5(b). Here one can see the significant difference between the groups. In Cellink Bioink, there was no visible formation of new larger vessels, yet there is newly formed tissue around the large vessels. The matrix remained intact and was not remodeled. For Alg/HA/Gel and Matrigel, where larger solid tumors formed, the formation of capillaries and hemorrhages in and around the tumor was visible. The tumors mainly grew at the chambers' entrance and replaced the hydrogels.

The serum was evaluated for MIA after 4 weeks of implantation (Cellink Bioink n = 7, Matrigel n = 5, Alg/HA/Gel n = 7). The MIA serum levels (Fig. 5(c)) were measurably increased in 3 animals of the Matrigel group and the Alg/HA/Gel group each after 4 weeks. These were the animals with the largest outgrown tumors. There was no significant difference between these two groups. In the Cellink Bioink group, no measurable increase was detectable.

3.5. Primary tumors have metastatic properties

To evaluate the metastatic phenotype of the explanted tumors, immunofluorescence stainings for MITF and BRN2, two factors involved in the regulation of proliferation, migration and metastasis of melanoma, and two further metastasis markers, ATX and MMP3, were performed.

Here, in Fig. 7(a), we could see the high expression of MITF but also the expression of BRN2 within the Mel Im tumors. There are some cells that have a higher BRN2 and lower MITF expression and vice versa. Microscopically, also cells with exclusively one of the two are detectable. Overall, the expression of the two markers within one tumor is heterogeneous. Furthermore, the tumors stain highly positive for ATX as well as MMP3 as shown in Fig. 7(b).

3.6. Lymph node metastases in Cellink Bioink

To evaluate the metastases of the tumors (Fig. 8) lymph nodes of the animals in the Cellink Bioink group were explanted (n = 6). Here, metastatic clusters were found in the *Lymphonodus subiliacus* (SiLN) and the *Lymphonodi iliaci mediales* (MILNs). The amount of metastases in the SiLN was significantly lower than in the MILNs. They insignificantly correlated with the Pearson correlation coefficient of 0.46 between the

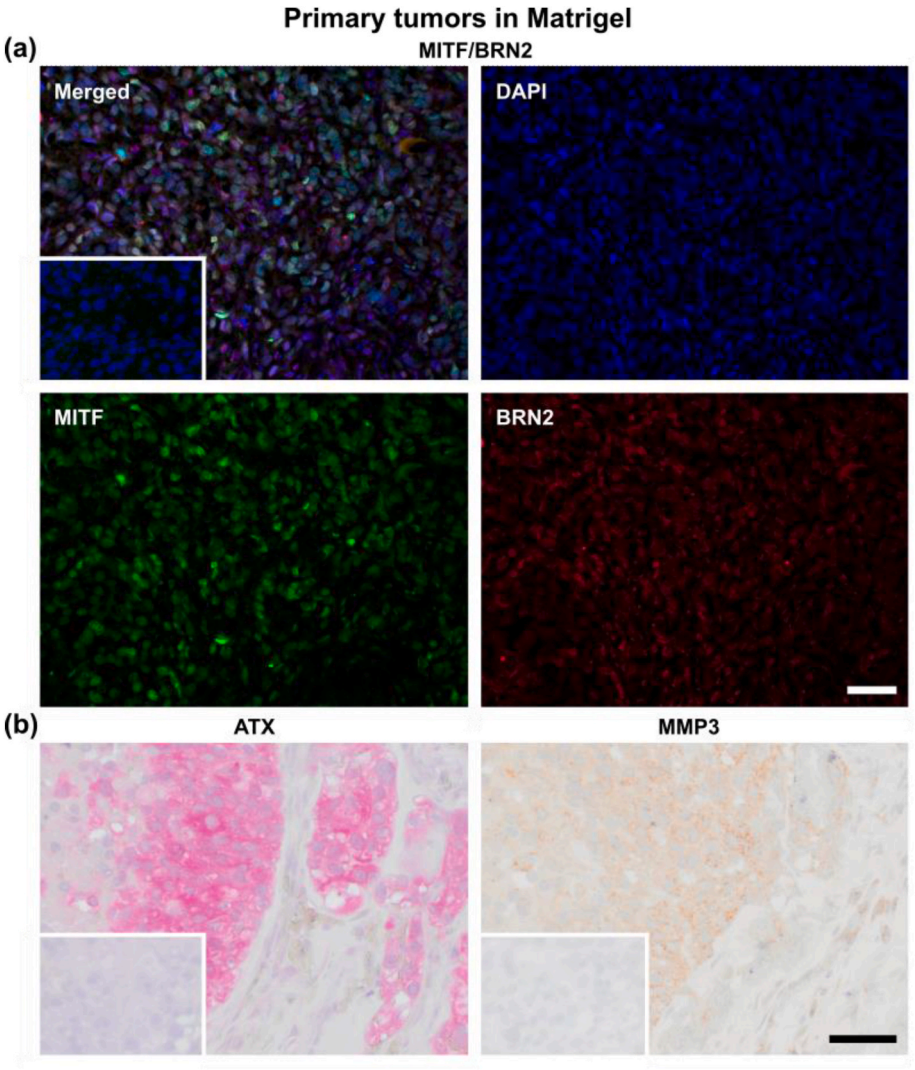

Fig. 7. Typical histology of primary melanoma explants as an example of the Matrigel group: (a) MITF and BRN2 immunofluorescent staining of one exemplary explant with expression of both MITF and BRN2 heterogeneously to slightly varying extents; **(b)** ATX and MMP3 immunohistological stainings of the tumor masses; controls without primary antibody are shown in the smaller boxes; scale bars = 50 μm.

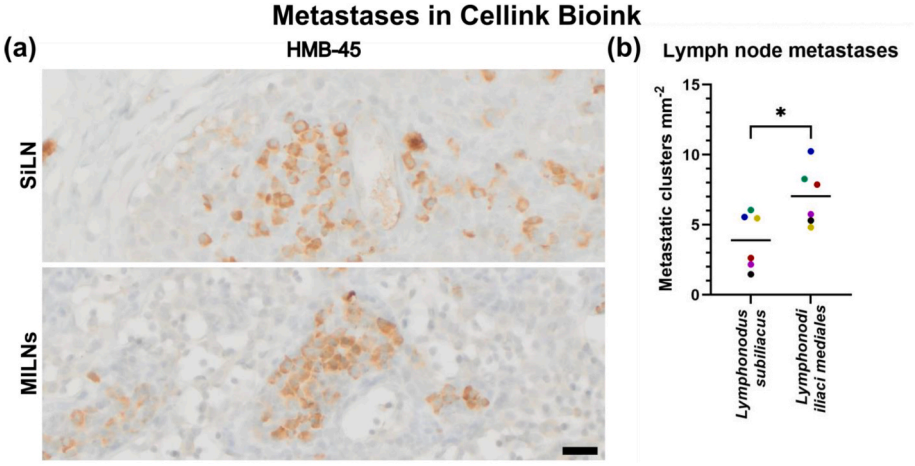

Fig. 8. Metastases in Cellink Bioink: (a): lymph node metastases of the Cellink Bioink group in *Lymphnodus subiliacus* (SiLN) and *Lymphnodi iliaci mediales* (MILNs), scale bar = 200 μm **(b)**: quantification of metastases in the lymph nodes shown as per animal color-coded individual values (with mean of ≥2 sections of biological replicates) plus mean of the group, *$p \leq 0.05$ (paired *t*-test).

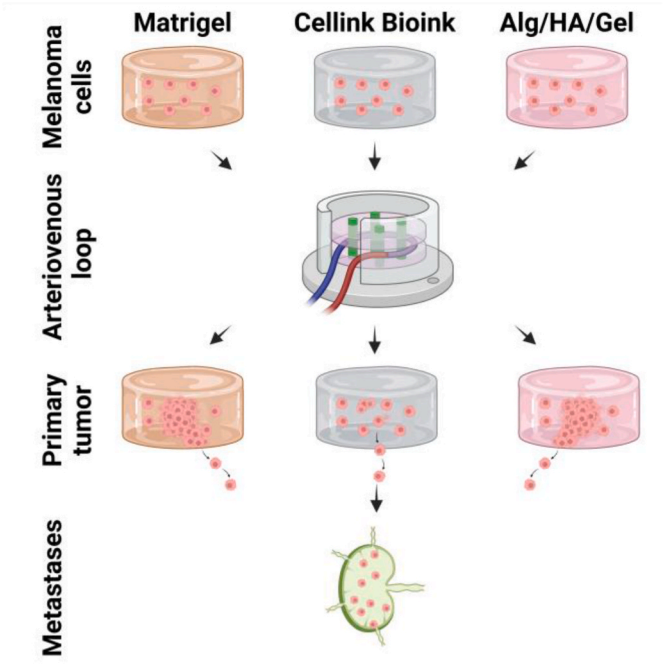

Fig. 9. ***In vivo*** **melanoma model:** three bioinks that highlight different tumor stages in the AV loop melanoma model.

two locations of the lymph nodes. In Fig. 8, representative histological stainings of the metastases in the lymph nodes are shown.

4. Discussion

With this study, we evaluated difference in tumor growth with fundamentally different bioinks that highlight different tumor stages (dormancy for Cellink Bioink and progression for Matrigel and Alg/HA/Gel) in a cast vascularized *in vivo* melanoma metastasis model (see Fig. 9) to establish the AV loop melanoma model as a robust tool for cancer research. Matrigel and Alg/HA/Gel both facilitate a good primary tumor growth while Cellink Bioink does not offer this possibility. Even without primary tumor growth, lymph node metastases can be found in the Cellink Bioink group.

Extrusion-based bioprinting has various advantages over standard hydrogel models. Theoretically, it offers the option to spatially arrange combinations of gels and cells in different concentrations in sophisticated macroporous structures and architectures. Not only is this of use for tissue engineering like skin substitutes [19], this makes it possible to further refine cancer models and precisely include cells from the tumor microenvironment [20] or perfusion systems that simulate blood flow. Examples of *in vitro* cancer research models are the inclusion of blood [21] or even lymphatic vessels [22] to study melanoma metastasis and therapy. With these approaches, also tumor spheroids can be printed and evaluated, better resembling small tumors. Biofabrication can futhermore be a versatile tool to create more defined tumor spheroids [23].

Here, the bioinks used can vary significantly and often are a very artificial non-physiological system, which has a tremendous effect on the microenvironment of the cells. Hence, it is important to evaluate the effect of the bioink used on the outcome of a model.

Matrigel, which is a standard matrix for various tumor models, is a basement membrane mix composed of type IV collagen, laminin, entactin, heparan sulfate proteoglycans, and various growth factors. Due to its mouse sarcoma origin, it has a typical pathophysiological tumor microenvironment. It facilitates substantial tumor proliferation but has limited transferability and use in humans due to its mouse sarcoma origin. due In contrast, Cellink Bioink is a for mammalian cells rather artificial microenvironment as it consists of alginate and cellulose nanofibrils with $CaCl_2$ as crosslinker. Although melanoma cells do survive the printing process and for longer time-periods *in vitro*, they are not capable of proliferating significantly within the matrix *in vitro* over 14 days [24]. This simulates a more dormant-like stage for tumor cells (Fig. 4), which was further evaluated in this study in an *in vivo* approach. Alg/HA/Gel, consisting of alginate, hyaluronic acid and gelatin with $CaCl_2$ as crosslinker, contains some components of the skin and is therefore closer to the human melanoma microenvironment than Cellink Bioink. It proved to be a versatile bioink with good printability and shape-fidelity, which are characterized more in this study, and additionally, it showed reliable *in vitro* and *in vivo* melanoma growth and tumor progression [7]. These explants were used as a reference in this study and expanded with further stainings and evaluations. The perspective of this study was to study the effect of the material and not the effect of the printing process onto the tumor growth; hence, printed constructs are planned for the future.

The printability and shape-fidelity differed massively between the three inks in this study. Rheology as well as printing tests (Fig. 2) attested the worst printability to Matrigel. Its low viscosity and additionally its high tan δ result in a low shape-fidelity after printing. For the use as a bioink, Matrigel shows limited suitability as it forms a temperature-dependent gel [24]. With standard extrusion-based printing techniques, it does not form defined structures. These limitations could be overcome using a support-bath assisted printing protocol where the support bath is removed after proper crosslinking of the Matrigel. These support baths have proven to be suitable for low-viscosity collagen bioinks [25].

The gelatin content of Alg/HA/Gel leads to stable strands at perfect printing conditions although over-gelation is possible when the ink is cooled too much [26]. The addition of stabilizing cellulose to the alginate in Cellink Bioink also increases shape-fidelity to a level where extrusion-based printing is feasible. Alg/HA/Gel had a higher DCR (0.59 ± 0.05) than Cellink Bioink (0.50 ± 0 03) and especially Matrigel (0.22 ± 0.04), confirming the best printability. The DCR is a good quantitative tool to measure shape-fidelity. The high DCR of Alg/HA/Gel and Cellink Bioink are comparable to other important inks [9] although also DCRs as high as 0.75 have been reported [27]. Cellink Bioink offers an almost similar printability to Alg/HA/Gel but not quite as good. Both are categorized as B in this study, which is better than other alginate-based inks [10]. Additionally, pre-crosslinking of alginate could further increase the shape-fidelity of alginate-based hydrogels [28]. The use of conical instead of cylindrical nozzles reduces the DCR [9] but decreases cell viability [29]. DCR and tan δ had a high correlation in this study.

Both, Alg/HA/Gel and Cellink Bioink showed a shear-thinning behavior that decreases cell death during printing. Nevertheless, cellular deformation when cells leave the nozzle cannot be neglected [30]. The addition of calcium to the bioink can decrease cell death [31]. Matrigel's low viscosity make shear stress effects on cells insignificant. It further creates the problem that cells settle down in the cartridge during printing and accumulate there.

The DMA (Fig. 3) proved that all the bioinks used form stable gels at 37 °C after gelation. Notably, Matrigel (43 ± 10.6 kPa) as well as Cellink Bioink (67.9 ± 7.3 kPa) have much higher storage moduli than Alg/HA/Gel (15.1 ± 0.9 kPa). Nevertheless, all of them are within the range of typical melanoma stiffness measurements, which are published in the range of 1.1–210 kPa [32]. Therefore, with regard to stiffness, all of the three bioinks can be valid models for melanoma research. Nevertheless, our results show that the tumor progression of our *in vivo* model is not stiffness dependent. This hypothesis has already been proven for further hydrogels [11]. Due to the composition of the bioinks, it is possible for the cells to interact with and bind to Matrigel and Alg/HA/Gel e. g. via RGD sequences to collagen/gelatin. HA additionally offers the possibility for CD44 interaction. In Cellink Bioink no integrin binding is possible by human cells.

SEM evaluation supported these findings. Although Matrigel has the least porous structure with only smallest pores (0.31 ± 0.11 μm), it is

still the most accessible to mammalian cells due to the possibility for degradation and remodeling. Alg/HA/Gel had an interconnected porous structure on day one. The free gelatin within the hydrogel seemed to diffuse into the medium, leaving a porous alginate backbone structure with pores that are 1.14 ± 0.18 μm in diameter. This offers the possibility for cells to form medium-sized colonies that displace the gel while not being able to degrade it and spread into it. Cellink Bioink had a similar pore size (1.42 ± 0.65 μm) with less than a tenth of the pore count of Alg/HA/Gel, making it impossible for cells to form larger colonies or migrate within the gel.

This has also an effect on the proliferation rate of cells (Fig. 4) within three days. In Cellink Bioink, this induces a dormant-like state of Mel Im with reduced Ki67 expression, comparable to previously published dormancy studies [33]. This effect is not based on the absence of cell anchorage as Mel Im can also form attachment-independent colonies from single cells [11]; this is a typical characteristic for tumor cells. This makes Cellink Bioink an interesting tool for cancer research as it offers an interesting microenvironment in which cells survive but do not proliferate. In Matrigel and Alg/HA/Gel, Ki67 expression is not reduced compared to the 2D culture. Here, colonies can form. In Alg/HA/Gel these Mel Im colonies are spherical without migration while in Matrigel, single cells can spread and migrate through the ECM-like hydrogel.

For the use in tissue engineering, various approaches to create vascularization have been established. One of these is the arteriovenous (AV) loop model [34–37]. It has been used for generating vascularized hard tissue (e. g. bone [38,39]) or soft tissue as well as lymphatic tissue [40]. The possible effective translation into clinical practice has also been demonstrated previously [41]. In this study, a closed chamber has been used. This promotes only intrinsic vascularization from the AV loop and makes it possible to study the interactions with the hydrogels in a more defined setting. Only through this route, nutrient supply and metastasis is possible. The advantage of the AV loop model in a closed chamber is that it is almost disconnected from the organism, making it more or less independent from the rat's microenvironment. This offers the possibility to study individual components of the microenvironment isolated from the others.

It is common for *in vivo* models to show variations between individuals. Not only the AV loop model itself has varying angiogenesis [42,43], also melanoma models have variations [44]. Therefore, our variations between animals are in an expected range. Overall, primary tumor growth (Fig. 5) for the Matrigel and the Cellink Bioink group were as anticipated from *in vitro* experiments [24]. Matrigel, as standard for many tumor models, is used for exactly this purpose. It is an ideal yet relatively undefined basis for the proliferation of many different cell types [45]. In Matrigel, large proliferative tumors formed that grew out of the chamber were found in all the animals. This was not observed with Cellink Bioink. In this regard, the Matrigel group performed even a little bit better than the Alg/HA/Gel group where only 7 out of 9 animals developed a tumor outside the chamber. The massive tumor growth was also verified histologically where Matrigel animals formed significantly larger tumors masses than the Cellink Bioink group. Fittingly, Matrigel had a larger average tumor area within the chambers than Alg/HA/Gel. Matrigel offers a better active degradability for mammalian cells than Cellink Bioink and Alg/HA/Gel as these cells do not have alginases to degrade alginate. Therefore, cell spreading is also best in Matrigel. There was one outlier detected in the tumor growth in the Cellink Bioink group. In the histology of this sample (data not shown), it appeared that there was a gap between the individual layers of the ink where a tumor could grow without the need to remodel the matrix. The filling of the chamber in layers of an opaque viscous matrix is difficult and the individual layers do not fuse during crosslinking. These gaps were filled by newly-formed tissue and could also lead to growth barriers. Therefore, a printed approach is superior to the layered technique used in this study and should be the standard approach for future studies.

What both groups with large proliferative tumors, Matrigel and Alg/HA/Gel, have in common is a high amount of hemorrhages both in histology and LSFM. These are a sign for a typical pathophysiological vasculature that is common for tumors with their continuous pro-angiogenic signaling and is poorly organized and leaky [46]. This leaky vasculature is an easy pathway for metastases. Besides the hemorrhages, LSFM for CD31 showed a dense capillary network of the tumors of Matrigel and Alg/HA/Gel. There were no vessels found within the three different matrices.

CD163 as inflammatory marker can also be used for melanoma prognosis [47,48]. Quantification of CD163 revealed a significant difference between Alg/HA/Gel and Cellink Bioink but not between Matrigel and Alg/HA/Gel. The average macrophage count in the Matrigel group tended to be higher than in Cellink Bioink. Macrophages were also found in the Matrigel and the Alg/HA/Gel within the gel without direct contact to the tissue. In Matrigel, mesenchymal migration with remodeling of the matrix is possible through the dense 3D structure without larger pores [49]. In Alg/HA/Gel they can migrate through the interconnected porous structure as macrophages can migrate through pores as small as 0.22 μm [50]. Even though macrophages can migrate without adhesion [51], they did not migrate into the Cellink Bioink. The material's pore count is too low to allow ameboid macrophage migration and without an attractant like a tumor mass, no infiltration was seen. Cellink Bioink is more inert to mammalian cells than the other materials, active degradation is not possible.

Melanoma Inhibitory Activity (MIA) is a potential melanoma marker [52]. In this study, the animals with the largest primary tumors also have a measurably elevated MIA level. Smaller tumors did not result in higher MIA within the serum. The reason on why the MIA ELISA in the Alg/HA/Gel group had higher minimal values is that they were performed with different standard curves. Hence, further comparisons for these low values are not reasonable. The values presumably are below the detection limit of the ELISA, as are the values in the Cellink Bioink group.

The explanted primary tumors have other typical metastatic melanoma properties (Figs. 6 and 7). Also in Cellink Bioink, metastatic cells can be found including cells in the endothelium. It is proposed that melanoma cells can switch their phenotype to a metastatic behavior [53]. Their expression of MITF and BRN2 show that some cells are primarily in a proliferative phenotype (high MITF expression) and others are in a migratory phenotype (high BRN2 expression) [54], while the explanted tumors are very heterogeneous within the tumor. ATX, a typical marker for multiple tumors is also found in melanomas; its expression is associated with melanoma proliferation and motility [55] and hence suggested to be involved in metastasis [56]. Accordingly, our explants showed high ATX expression by the tumors. Further, high expression of MMP3 is associated with worse survival in metastatic melanoma [57]. The explanted tumors grown from the metastatic cell line Mel Im showed high levels of this MMP.

Surprisingly, although primary tumor growth was almost non-existent in Cellink Bioink, metastatic clusters were found in all lymph nodes examined. Even in this group, a metastatic phenotype is possible. This effect could be triggered by the differences in stiffness of the hydrogels as increased stiffness also increases invasion and metastasis rates of cancer cells [58]. This effect should also be independent from integrin bidning [59]. Further studies are necessary to verify these hypotheses. MITF expression and therefore invasiveness is stronly influenced by the tumor microenvironment [53] and in this case the bioink.

As expected, the amount of lymph node metastases was higher in the lymph nodes closer to the draining vein of the AV loop, the MILNs, than in the SiLNs. The presence of nodal melanoma metastasis is regarded as a critical factor for treatment and is seen by some as a marker for the metastatic potential and as an incubator for progression and metastasis for others [60]. Within this study, all of the metastases were in an early stage and not palpable or visible macroscopically. For future studies it is highly interesting to evaluate other organs as well.

Specific modifications to the bioinks (e. g. stiffness changes, specific matrix protein or cytokine inclusion, co-cultures with cells from the

tumor microenvironment like stem cells or cancer-associated fibroblasts) could alter the cellular response and give further information on pathophysiological processes. RNA sequencing of melanoma cells in Cellink Bioink could provide an insight on the phenotype of these cells in a dormant state, when comparing it to a proliferation ink like Alg/HA/Gel. Using 3D biofabrication, it is possible to combine the materials in interesting settings. E. g. a core of melanoma cells in a proliferation ink, surrounded by a ring of Cellink Bioink, inside more proliferation ink could give insight on the switch from a dormant to a proliferative state and vice versa at the interphases of the gels.

5. Conclusion

Three fundamentally different bioinks, Matrigel, Cellink Bioink, and Alg/HA/Gel, that mimic different tumor stages *in vitro*, led to significantly different primary tumor growth in the vascularized *in vivo* melanoma model used. It was possible to mimic progression (Matrigel and Alg/HA/Gel) as well as dormancy (Cellink Bioink) states of tumors in a defined microenvironment in an isolated chamber with defined interaction with the organism via the AV loop. Interestingly, metastasis was also possible even without primary tumor growth. Human-like metastasis originiating from different tumor stages can be studied with all the bioinks. These findings show that this novel AV loop melanoma model is very robust and can be used to further study molecular aspects and therapies.

Ethics approval and consent to participate

These experiments were approved by the Animal Care Committee of the University Erlangen-Nürnberg (FAU) and the Government of Unterfranken, Germany (license number 55.2-2532-2-718).

Funding

The work was funded by the Deutsche Forschungsgemeinschaft (DFG, German Research Foundation), Project number 326998133, TRR 225 (subprojects C03, A07, C04, and Z03).

CRediT authorship contribution statement

Rafael Schmid: Writing – review & editing, Writing – original draft, Visualization, Methodology, Investigation. **Sonja K. Schmidt:** Writing – review & editing, Writing – original draft, Investigation. **Stefan Schrüfer:** Writing – review & editing, Investigation. **Dirk W. Schubert:** Writing – review & editing, Investigation. **Stefanie Heltmann-Meyer:** Writing – review & editing, Writing – original draft, Investigation. **Martin Schicht:** Investigation. **Friedrich Paulsen:** Investigation. **Raymund E. Horch:** Writing – review & editing, Writing – original draft, Resources, Methodology. **Anja K. Bosserhoff:** Writing – review & editing, Writing – original draft, Supervision, Funding acquisition, Conceptualization. **Annika Kengelbach-Weigand:** Writing – review & editing, Writing – original draft, Supervision, Funding acquisition, Conceptualization. **Andreas Arkudas:** Writing – review & editing, Writing – original draft, Supervision, Funding acquisition, Conceptualization.

Declaration of competing interest

The authors declare that they have no known competing financial interests or personal relationships that could have appeared to influence the work reported in this paper.

Data availability

Data will be made available on request.

Acknowledgements

We would like to thank Stefan Fleischer, Ilse Arnold-Herberth, Marina Milde, Sheetal Kadam, Andrea Beck, Christina Fischer, Andrea Eichhorn, and Elke Kretzschmar for their excellent technical support.

References

[1] F. Tas, Metastatic behavior in melanoma: timing, pattern, survival, and influencing factors, JAMA Oncol. 2012 (2012) 647684.
[2] E. Hirata, E. Sahai, Tumor microenvironment and Differential responses to therapy, Cold Spring Harb Perspect Med 7 (7) (2017).
[3] N. Nagarsheth, M.S. Wicha, W. Zou, Chemokines in the cancer microenvironment and their relevance in cancer immunotherapy, Nat. Rev. Immunol. 17 (9) (2017) 559–572.
[4] M. Kappelmann-Fenzl, et al., Molecular changes induced in melanoma by cell culturing in 3D alginate hydrogels, Cancers (Basel) 13 (16) (2021).
[5] B. Yao, et al., Enzymatically degradable alginate/gelatin bioink promotes cellular behavior and degradation in vitro and in vivo, Biofabrication 11 (4) (2019) 045020.
[6] C. Antich, et al., Bio-inspired hydrogel composed of hyaluronic acid and alginate as a potential bioink for 3D bioprinting of articular cartilage engineering constructs, Acta Biomater. 106 (2020) 114–123.
[7] R. Schmid, et al., A new printable alginate/hyaluronic acid/gelatin hydrogel suitable for biofabrication of in vitro and in vivo metastatic melanoma models, Adv. Funct. Mater. 32 (2) (2021).
[8] A. Weigand, et al., The arteriovenous loop: engineering of axially vascularized tissue, Eur. Surg. Res. 59 (3–4) (2018) 286–299.
[9] J. Schulik, et al., Comparison of the behavior of 3D-printed endothelial cells in different bioinks, Bioengineering 10 (7) (2023).
[10] J. Hazur, et al., Pre-crosslinking with hydrogel microparticles enhances the printability of alginate-based inks, Macromol. Mater. Eng. 308 (12) (2023).
[11] R. Schmid, et al., Comparison of hydrogels for the development of well-defined 3D cancer models of breast cancer and melanoma, Cancers (Basel) 12 (8) (2020).
[12] J. Schindelin, et al., Fiji: an open-source platform for biological-image analysis, Nat. Methods 9 (7) (2012) 676–682.
[13] J.P. Johnson, et al., Surface antigens of human melanoma cells defined by monoclonal antibodies. I. Biochemical characterization of two antigens found on cell lines and fresh tumors of diverse tissue origin, Eur. J. Immunol. 11 (10) (1981) 825–831.
[14] A. Weigand, et al., The arteriovenous (AV) loop in a small animal model to study angiogenesis and vascularized tissue engineering, J. Vis. Exp. 117 (2016).
[15] A. Klingberg, et al., Fully automated evaluation of total glomerular number and capillary tuft size in nephritic kidneys using lightsheet microscopy, Journal of the Amercian Society of Nephrology 28 (2017) 452–459.
[16] A. Grüneboom, et al., A network of trans-cortical capillaries as mainstay for blood circulation in long bones, Nat. Metab. 1 (2) (2019) 236–250.
[17] R. An, et al., Proangiogenic effects of tumor cells on endothelial progenitor cells vary with tumor type in an in vitro and in vivo rat model, Faseb. J. 32 (10) (2018) 5587–5601.
[18] S. Heltmann-Meyer, et al., Gelatin methacryloyl is a slow degrading material allowing vascularization and long-term usein vivo, Biomed. Mater. 16 (6) (2021).
[19] C.A. Sorgel, et al., Perspectives on the current state of bioprinted skin substitutes for wound healing, Biomedicines 11 (10) (2023).
[20] H. Horder, et al., Bioprinting and differentiation of adipose-derived stromal cell spheroids for a 3D breast cancer-adipose tissue model, Cells 10 (4) (2021).
[21] B.S. Kim, et al., Construction of tissue-level cancer-vascular model with high-precision position control via in situ 3D cell printing, Small Methods 5 (7) (2021) e2100072.
[22] W.W. Cho, et al., Blood-lymphatic integrated system with heterogeneous melanoma spheroids via in-bath three-dimensional bioprinting for modelling of combinational targeted therapy, Adv. Sci. 9 (29) (2022) e2202093.
[23] P. Zhuang, et al., Using spheroids as building blocks towards 3D bioprinting of tumor microenvironment, Int J Bioprint 7 (4) (2021) 444.
[24] S.K. Schmidt, et al., Tumor cells develop defined cellular phenotypes after 3D-bioprinting in different bioinks, Cells 8 (10) (2019).
[25] T.U. Esser, et al., Direct 3D-bioprinting of hiPSC-derived cardiomyocytes to generate functional cardiac tissues, Adv. Mater. (2023) e2305911.
[26] L. Ouyang, et al., Effect of bioink properties on printability and cell viability for 3D bioplotting of embryonic stem cells, Biofabrication 8 (3) (2016) 035020.
[27] V. Bednarzig, et al., Improved 3D printing and cell biology characterization of inorganic-filler containing alginate-based composites for bone regeneration: particle shape and effective surface area are the dominant factors for printing performance, Int. J. Mol. Sci. 23 (9) (2022).
[28] J. Hazur, et al., Improving alginate printability for biofabrication: establishment of a universal and homogeneous pre-crosslinking technique, Biofabrication 12 (4) (2020) 045004.
[29] R. Chand, B.S. Muhire, S. Vijayavenkataraman, Computational fluid dynamics assessment of the effect of bioprinting parameters in extrusion bioprinting, Int J Bioprint 8 (2) (2022) 545.
[30] S.J. Müller, B. Fabry, S. Gekle, Predicting cell stress and strain during extrusion bioprinting, Phys. Rev. Appl. 19 (6) (2023).
[31] L. Fischer, et al., Calcium supplementation of bioinks reduces shear stress-induced cell damage during bioprinting, Biofabrication 14 (4) (2022).

[32] H. Joodaki, M.B. Panzer, Skin mechanical properties and modeling: a review, Proc. Inst. Mech. Eng. H 232 (4) (2018) 323–343.
[33] H.F. Aqbi, et al., Local and distant tumor dormancy during early stage breast cancer are associated with the predominance of infiltrating T effector subsets, Breast Cancer Res. 22 (1) (2020) 116.
[34] R. Vaghela, et al., Microvascular development in the rat arteriovenous loop model in vivo-A step by step intravital microscopy analysis, J. Biomed. Mater. Res. 110 (9) (2022) 1551–1563.
[35] R. An, et al., An innovative arteriovenous (AV) loop breast cancer model tailored for cancer research, Bioengineering (Basel) 9 (7) (2022).
[36] S. Kratzer, et al., Vascularization of poly-ε-caprolactone-collagen I-nanofibers with or without sacrificial fibers in the neurotized arteriovenous loop model, Cells 11 (23) (2022).
[37] R. Vaghela, et al., A novel window into angiogenesis-intravital microscopy in the AV-loop-model, Cells 12 (2) (2023).
[38] S. Winkler, et al., Human umbilical vein endothelial cell support bone formation of adipose-derived stem cell-loaded and 3D-printed osteogenic matrices in the arteriovenous loop model, Tissue Eng Part A. 27 (5-6) (2021 Mar) 413–423, https://doi.org/10.1089/ten.TEA.2020.0087.
[39] A.M. Boos, et al., Engineering axially vascularized bone in the sheep arteriovenous-loop model, Journal of Tissue Engineering and Regenerative Medicine 7 (8) (2013) 654–664.
[40] J.W. Robering, et al., Tissue engineering of lymphatic vasculature in the arteriovenous loop model of the rat, Tissue Eng. 27 (1–2) (2021) 129–141, https://doi.org/10.1089/ten.TEA.2020.0108.
[41] R.E. Horch, et al., Successful human long-term application of in situ bone tissue engineering, J. Cell Mol. Med. 18 (7) (2014) 1478–1485.
[42] A. Arkudas, et al., Dose-finding study of fibrin gel-immobilized vascular endothelial growth factor 165 and basic fibroblast growth factor in the arteriovenous loop rat model, Tissue Eng. 15 (9) (2009) 2501–2511.
[43] A. Arkudas, et al., Fibrin gel-immobilized VEGF and bFGF efficiently stimulate angiogenesis in the AV loop model, Mol. Med. 13 (9–10) (2007) 480–487.
[44] C.W. Stackpole, Distinct lung-colonizing and lung-metastasizing cell populations in B16 mouse melanoma, Nature 289 (5800) (1981) 798–800.
[45] O. Habanjar, et al., 3D cell culture systems: tumor application, advantages, and disadvantages, Int. J. Mol. Sci. 22 (22) (2021).
[46] M.B. Schaaf, A.D. Garg, P. Agostinis, Defining the role of the tumor vasculature in antitumor immunity and immunotherapy, Cell Death Dis. 9 (2) (2018) 115.
[47] T.O. Jensen, et al., Macrophage markers in serum and tumor have prognostic impact in American Joint Committee on Cancer stage I/II melanoma, J. Clin. Oncol. 27 (20) (2009) 3330–3337.
[48] S. Salmi, et al., The number and localization of CD68+ and CD163+ macrophages in different stages of cutaneous melanoma, Melanoma Res. 29 (3) (2019) 237–247.
[49] I. Maridonneau-Parini, Control of macrophage 3D migration: a therapeutic challenge to limit tissue infiltration, Immunol. Rev. 262 (1) (2014) 216–231.
[50] A. Stevens, M. Bahr, Origin of macrophages in central nervous tissue. A study using intraperitoneal transplants contained in Millipore diffusion chambers, J. Neurol. Sci. 118 (2) (1993) 117–122.
[51] A.N. Rumianek, D.R. Greaves, How have leukocyte in vitro chemotaxis assays shaped our ideas about macrophage migration? Biology 9 (12) (2020).
[52] A.K. Bosserhoff, et al., Melanoma inhibitory activity (MIA), a serological marker of malignant melanoma, Recent Results Cancer Res. 158 (2001) 158–168.
[53] K.S. Hoek, C.R. Goding, Cancer stem cells versus phenotype-switching in melanoma, Pigment Cell Melanoma Res 23 (6) (2010) 746–759.
[54] M.P. Smith, et al., A PAX3/BRN2 rheostat controls the dynamics of BRAF mediated MITF regulation in MITFhigh/AXL(low) melanoma, Pigment Cell & Melanoma Research 32 (2) (2019) 280–291.
[55] M. Umezu-Goto, et al., Autotaxin has lysophospholipase D activity leading to tumor cell growth and motility by lysophosphatidic acid production, J. Cell Biol. 158 (2) (2002) 227–233.
[56] M. Jankowski, Autotaxin: its role in biology of melanoma cells and as a pharmacological target, Enzym. Res. 2011 (2011) 194857.
[57] J. Nikkola, et al., High expression levels of collagenase-1 and stromelysin-1 correlate with shorter disease-free survival in human metastatic melanoma, Int. J. Cancer 97 (4) (2002) 432–438.
[58] Y. Jiang, et al., Targeting extracellular matrix stiffness and mechanotransducers to improve cancer therapy, J. Hematol. Oncol. 15 (1) (2022) 34.
[59] X. Tang, et al., Mechanical force affects expression of an in vitro metastasis-like phenotype in HCT-8 cells, Biophys. J. 99 (8) (2010) 2460–2469.
[60] M.B. Faries, et al., Lymph node metastasis in melanoma: a debate on the significance of nodal metastases, conditional survival analysis and clinical trials, Clin. Exp. Metastasis 35 (5–6) (2018) 431–442.